Catalytic oxidation of linalool with Keggin POMs: Insights into homogeneous vs. heterogeneous approaches

Ali Al Hadi Haidar, Sonia Mallet-Ladeira, Pascal Guillo, Dominique Agustin

▶ **To cite this version:**

Ali Al Hadi Haidar, Sonia Mallet-Ladeira, Pascal Guillo, Dominique Agustin. Catalytic oxidation of linalool with Keggin POMs: Insights into homogeneous vs. heterogeneous approaches. Applied Catalysis O: Open, 2025, 208, pp.207074. ⟨10.1016/j.apcato.2025.207074⟩. ⟨hal-05582168⟩

HAL Id: hal-05582168

https://hal.science/hal-05582168v1

Submitted on 7 Apr 2026

HAL is a multi-disciplinary open access archive for the deposit and dissemination of scientific research documents, whether they are published or not. The documents may come from teaching and research institutions in France or abroad, or from public or private research centers.

L'archive ouverte pluridisciplinaire **HAL**, est destinée au dépôt et à la diffusion de documents scientifiques de niveau recherche, publiés ou non, émanant des établissements d'enseignement et de recherche français ou étrangers, des laboratoires publics ou privés.

Distributed under a Creative Commons CC BY-NC-ND 4.0 - Attribution - Non-commercial use - No Derivative Works - International License

Applied Catalysis O: Open 208 (2025) 207074

Contents lists available at ScienceDirect

Applied Catalysis O: Open

journal homepage: www.elsevier.com/locate/apcato

Catalytic oxidation of linalool with Keggin POMs: Insights into homogeneous vs. heterogeneous approaches☆

Ali Al Hadi Haidar [a], Sonia Mallet-Ladeira [a,b], Pascal Guillo [a,c], Dominique Agustin [a,c,*]

[a] LCC-CNRS, Université de Toulouse, CNRS, Toulouse, France
[b] Institut de Chimie de Toulouse (ICT, UAR 2599), 118 Route de Narbonne, 31062 Toulouse Cedex 09, France
[c] Department of Chemistry, Institut Universitaire de Technologie Toulouse Auch Castres, University of Toulouse, 5 allée du Martinet, F-81100 Castres, France

ARTICLE INFO

Keywords:
Polyoxometalates
Linalool
Biomass valorisation
Oxidation
Silica supported catalyst
Organic solvent-free protocol

ABSTRACT

This study explores the catalytic performance of molybdenum (Mo)- and vanadium (V)- containing Keggin polyoxometalates (POMs) of general formula $(PMo_{12-x}V_xO_{40})^{(3+x)-}$ (x = 0,1,2). The studied molecular complexes bear protons (HPAs) or organic cations such as butylpyridinium (BuPyr), 1-butyl-3-methylimidazolium (BmIm), and tetrabutylammonium (TBA). POMs were also ionically immobilized on silica beads functionalized with 1-methylimidazolium or pyridinium moieties, enabling catalyst recovery and recycling. HPAs, molecular POMs and immobilized ones were evaluated as catalysts for the oxidation of linalool towards pyranoid (**P**) and furanoid (**F**) using hydrogen peroxide (H_2O_2) or *tert*-butyl hydroperoxide (TBHP) as oxidants. With 0.25 % POM/substrate molar ratio, some heterogeneous systems demonstrated high catalytic efficiency (80 % conversion) and up to 70 % selectivity towards **F** + **P** products over four consecutive runs. Different parameters were studied including organic solvent-free processes, recycling tests and green metrics.

1. Introduction

Oxidation reactions are essential transformations in the vast landscape of chemical processes. The applications of resulting products range from energy production to the synthesis of valuable products in industries such as pharmaceuticals, agrochemicals, and materials science [1]. For example, oxidation of alcohols into aldehydes or ketones is crucial in both laboratory-scale research and large-scale industrial production [2]. Historically, these reactions have been carried out under harsh conditions, usually requiring stoichiometric amounts of toxic metal-based oxidants such as chromium [3,4] or permanganate salts [5], chlorinated solvents [6], and elevated parameters such as temperatures or pressure [7]. This results in the generation of substantial chemical waste, including hazardous byproducts which pose serious environmental and health risks [8].

In recent decades, chemistry has shifted towards greener and more sustainable methods [9,10]. Among them, most of the energy-sober processes used catalysis. Catalytic oxidation systems, particularly those using metal-based catalysts, have garnered much attention for their ability to reduce waste and energy consumption by employing milder, greener conditions. The transition from traditional non-green oxidants to greener alternatives such as molecular oxygen O_2 [11,12], hydrogen peroxide (H_2O_2) [13], and *tert*-butyl hydroperoxide (TBHP) [14] has become a central focus in the development of oxidation reactions. However, activating these oxidants under mild conditions while maintaining high efficiency and selectivity remains a significant challenge [15]. Another major goal in the field of "green chemistry" is to find an alternative to chemicals based on fossil resources as starting reagents [16]. One promising approach involves the use of biomass-derived substrates, such as terpenes, providing renewable, natural alternatives to fossil-based chemicals. In this context, terpenols are among the targeted substrates that can lead to high value compounds [17]. The present work focused on the synthesis of furanoid (**F**) and pyranoid (**P**) scaffolds (Scheme 1). Those two molecules are valuable compounds in drug synthesis and biological applications [18,19]. In recent years, these building blocks, have been classically synthesized through 5-hexenol ring closure or reactions between homoallylic alcohols and aldehydes for example (Scheme 1, left and right) [20,21]. They can also be synthesized directly from Linalool (**L**), a biomass based substrate, using peracetic acid or *m*-CPBA in toxic solvents such as dichloromethane (Scheme 1, middle) [22,23]. However, all these methods generated substantial waste.

☆ This article is part of a Special issue entitled: 'APCATSTARS' published in Applied Catalysis O: Open.

* Corresponding author at: LCC-CNRS, Université de Toulouse, CNRS, Toulouse, France.
E-mail address: dominique.agustin@iut-tlse3.fr (D. Agustin).

https://doi.org/10.1016/j.apcato.2025.207074
Received 30 July 2025; Received in revised form 1 September 2025; Accepted 10 September 2025
Available online 13 September 2025
2950-6484/© 2025 The Authors. Published by Elsevier B.V. This is an open access article under the CC BY-NC-ND license (http://creativecommons.org/licenses/by-nc-nd/4.0/).

Interestingly, in 2020, Villanculo et al. reported the 1-step synthesis of compounds **F** and **P** from linalool, using hydrogen peroxide as the oxidant and acetonitrile as the solvent, in the presence of a lacunary Keggin-type catalyst [24] (Scheme 1, middle). Under these conditions, combined yields of **F** and **P** ranged from 40 % to 80 %, with best results obtained using a 0.33 mol% catalyst loading. This greener approach, based on a biomass-derived starting material, was also validated by our group, employing molybdenum and vanadium Schiff base coordination complexes as catalysts, achieving higher yields of **F** and **P**, ranging from 8 % to 85 % [25].

Our research focuses on the development of recyclable catalytic systems for biomass-derived substrates. Polyoxometalates (POMs), a class of metal-oxygen clusters known for structural stability, tunable redox properties, acidity, and solubility in various media, have attracted considerable attention due to their ability to activate mild oxidants such as H_2O_2 and TBHP [26], making them ideal candidates for oxidation reactions [11,12]. Among the various strategies for POM recovery and reuse, two approaches emerged: the formulation of POM-based ionic salts [27–29] and the heterogenization of POMs onto solid supports [30–32]. The combination of POMs with organic cations offers a synergistic enhancement of their respective properties, improving performance and versatility, particularly in oxidation catalysis. For heterogeneous systems, amorphous silica is preferred as support due to its thermal stability, commercial availability and ease of functionalization [32,33].

Based on previous works on Merrifield resin as a support for POMs [34,35], highlighting the superior activity of mixed Mo/V POMs [35], and the successful ionic grafting of POMs onto modified silica surfaces [31,32,36], the present study reports the green oxidation of linalool into **F** and **P** using both homogeneous and heterogeneous POM-based catalytic systems. We compare herein the reactivity of three synthesized POMs $(PMo_{12-x}V_xO_{40})^{(3+x)-}$ (x = 0,1,2) in combination with several organic cations, tetrabutylammonium (TBA), 1-butyl-pyridinium (BP), and butylmethylimidazolium (BmIm). For heterogeneous catalysis, silica-supported POMs were prepared via surface functionalization. Efficiency, recovery, and reusability of these systems under solvent-free conditions are evaluated, with particular attention to the selectivity towards targeted derivatives using aqueous TBHP and H_2O_2 as oxidants.

2. Experimental

2.1. Materials

All materials were used without further purification. Organic solvents: (Acetonitrile, ethanol, methanol, diethyl ether, toluene, pyridine), Linalool (96 %, TCI), 2-(5-methyl-5- vinyltetrahydro-furan-2-yl propan-2-ol) (97 %, Aldrich), 2,2,6-Trimethyl-6-vinyltetrahydropyran-3-ol (98 %, TCI), H_2O_2 (35 %, ACROS), $TBHP_{aq}$ (70 % TBHP in water, ACROS), dodecane (99 %, Aldrich), Molybdatophosphoric acid hydrate (Merck) denoted as $H_3PMo_{12}O_{40}$, Sodium-molybdate dihydrate (99 %, THERMO SCIENTIFIC), Sodium metavanadate (Alfa Aesar), Disodium phosphate (Acros 99 %), Sulfuric acid (95 %, Sigma Aldrich), 1-butyl pyridinium bromide (Fluka 99 %), Butyl methyl imidazolium chloride (synthesized) [37], 1-methyl imidazole (Acros 99 %), Tetrabutylammonium bromide (Acros 99 %), TEOS (tetraethyl orthosilicate) (Merck), Ammonia solution (Sigma Aldrich 28 %), Chloropropyl triethoxysilane (TCI 97 %) were used as received.

2.2. Methods

Powder X-ray diffraction: The solids were analyzed by X-ray diffraction (XRD) with a Bruker (Karlsruhe, Germany) D2 X'Pert PRO diffractometer using Cu Kα radiation (40 kV and 40 mA).

Dynamic Light Scattering (DLS): Particle samples were prepared in water or methanol. Sonication of particles suspension was made before DLS analysis during 10 min facilitating the dispersion of silica particles. Hydrodynamic diameters of the particles in suspension were obtained with a ZetaSizer Nano-ZS (Malvern Instruments Ltd., Worcestershire, UK,) at 25 °C. This equipment uses a laser (He—Ne at λ = 633 nm, under voltage of 3 mV) and the detector was located at 173° to analyze the scattered intensity fluctuations.

Solution NMR: ^{1}H NMR, ^{13}C{^{1}H}-NMR and ^{31}P{^{1}H}-NMR spectra were recorded on Bruker (Fällanden, Switzerland) NMR III HD 400 MHz spectrometers. 400 MHz for ^{1}H NMR, 101 MHz for ^{13}C NMR and 162 MHz for ^{31}P NMR. ^{1}H and ^{13}C chemical shifts (δ) are reported in ppm vs. $SiMe_4$ and were determined using the residual ^{1}H and ^{13}C solvent peaks as internal standards. The coupling constants are reported in Hertz.

Solid state NMR: Solid state NMR: MAS NMR experiments were recorded on Bruker Avance (Fällanden, Switzerland) 400 III HD spectrometers operating at magnetic fields of 9.4 T. Samples were packed into 4 mm zirconia rotors. The rotors were spun at 8 kHz at 293 K. ^{1}H MAS was performed with DEPTH pulse sequence and a relaxation delay of 3 s. For ^{29}Si MAS single pulse experiments, small flip angle of 30° were used with a recycle delays of 60 s. ^{13}C CP and ^{29}Si CP MAS spectra were recorded with a recycle delay of 2 s and contact times of 3 ms and 4 ms, respectively. Chemical shifts were referenced to TMS. All spectra were fitted using the DMfit software (version 20,190,125).

EDX-SEM: EDX-SEM experiments were recorded using JSM-7800F Prime machine performed by service de Microscopie Électronique - LCC CNRS Toulouse.

Elemental analysis: The elemental analyses were carried out by the analytical service of the LCC-Toulouse by using a PerkinElmer 2400 CHNS/O Series II System (100 V).

ATR-Infrared (ATR-IR) spectra were recorded using the ATR

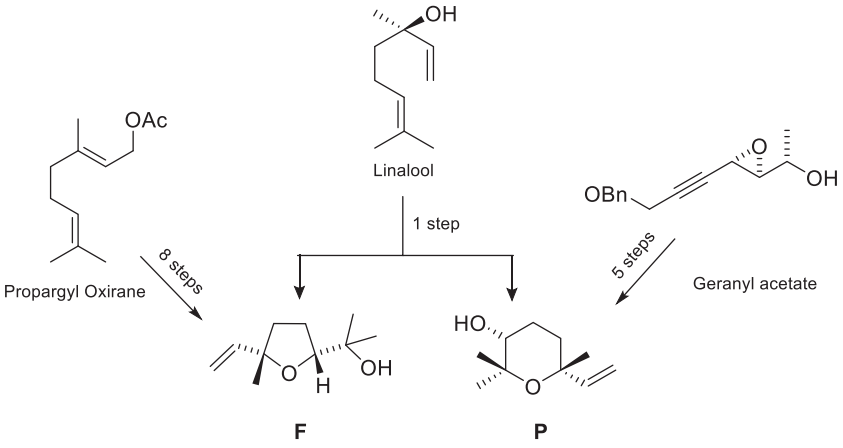

Scheme 1. Synthesis of **F** from propargyl oxirane (left), Synthesis of **P** from geranyl acetate (right) and **F** and **P** Synthesis from Linalool (middle)

technique with a Perkin Elmer FTIR/FIR 400 spectrometer.

Quantification of the number of POMs per gram of grafted silica through $^{31}P\{^{1}H\}$ NMR in solution: 5 mg of **SiO_2@PM** was added in 4 mL of D_2O/NaOH solution (pH ≈ 13) in an NMR tube. The mixture was heated until the powder completely dissolved. The PM amount per gram of the **SiO_2@PM** sample was calculated from calibration curves (r^2 = 0.999) obtained with different concentrations on phosphates at the same pH considering the ^{31}P NMR shift around −4.7 ppm.

Centrifugation: The silica beads were collected by centrifugation on a Sigma 2-16P with 11,192 rotor (Max. rpm 4500, Sigma, Osterode am Harz, Germany).

Gas chromatography: The catalytic reactions were followed by gas chromatography (GC) on an Agilent 7820 A chromatograph equipped with an FID detector, a DB-WAX capillary column (30 m × 0.32 mm × 0.5 μm) and autosampler. **L** conversion and **F** and **P** formation were calculated from the calibration curves (r^2 = 0.999) and dodecane as internal standard. All parameters of the reactions were deduced from those measurements. The exact definitions of TON and TOF are given in footnotes of each Table.

X-ray structural analyses: Single crystal of **$(BmIm)_3PMo_{12}$** was mounted on a MiTeGen MicroLoop using perfluoropolyether oil. Data were collected on a Rigaku XtaLAB Synergy Dualflex diffractometer using a PhotonJet X-ray source (MoKα, λ = 0.71073 Å). An Oxford Cryosystems Cryostream cooling device was used to collect data at low temperature (100(2) K). Omega scans were performed for data collection. An empirical absorption correction was applied and the structures were solved by intrinsic phasing method (ShelXT) [38]. All non-hydrogen atoms were refined anisotropically by means of least squares procedures on F^2 with ShelXL [39]. All the hydrogen atoms were refined isotropically at calculated positions using a riding model. ORTEP views of the asymmetric units of the crystal structures with labeling of all non-H atoms, and tables giving crystal data and structure refinement parameters are available in the ESI.

Crystallographic data (excluding structure factors) have been deposited with the Cambridge Crystallographic Data Centre as supplementary publication no. CCDC 2475932. Copies of the data can be obtained free of charge on application to the Director, CCDC, 12 Union Road, Cambridge CB2 1EZ, UK (fax: (+44) 1223–336-033; e-mail: deposit@ccdc.cam.ac.uk).

2.3. Preparation of catalytic components

2.3.1. Synthesis of heteropolyacids (HPAs)

$H_4PMo_{11}V_1O_{40}$ and $H_5PMo_{10}V_2O_{40}$ were synthesized according to the published procedure [40]. ATR-IR for the three HPAs. $\nu(cm^{-1})$: 1055–1100 (P—O), 1000–900 (M-O), 850–700 (M-O-M). $H_3PMo_{12}O_{40}$: $^{31}P\{^{1}H\}$ NMR (162 MHz, DMSO-d_6) δ (ppm) = −0.5 (minor), −4 (major). $H_4PMo_{11}V_1O_{40}$: $^{31}P\{^{1}H\}$ NMR (162 MHz, DMSO-d_6) δ (ppm) = −1, −4.11. $H_5PMo_{10}V_2O_{40}$: $^{31}P\{^{1}H\}$ NMR (162 MHz, DMSO-d_6) δ (ppm) = −1 (minor), −4.5 (major).

2.3.2. General synthesis of organic salts of POMs

Organic Salts of POMs were synthesized by mixing the corresponding HPA with x equivalent of tetrabutylammonium bromide, butylmethylimidazolium chloride, or 1-butylpyridinium bromide in water. The precipitated salts were filtered, washed with water then dried. Syntheses of **$(BmIm)_3PMo_{12}$**, **$(BmIm)_4PMo_{11}V$**, **$(BuPyr)_3PMo_{12}$** and **$(BuPyr)_4PMo_{11}V$** have already been reported [35]. Only syntheses of new compounds are reported in this manuscript.

$(BmIm)_5PMo_{10}V_2$: $H_5PMo_{10}V_2O_{40}.31H_2O$ (1 g, 0.43 mmol) was mixed with 1-butyl-3-methyl imidazolium chloride (0.47 g, 2.1 mmol) in 10 mL water at room temperature for 4 h. The orange salt formed was filtered and dried under vacuum. Yield: 91 %. Elem. Anal. Calc: C, 19.70; H, 3.11; N, 5.77. Found: C, 19.78; H, 3.11, N, 5.00. ATR-IR ν (cm^{-1}): 3150–2850 (CH), 1564 (C=C), 1463 (C—N), 1061 (P—O), 955 (Mo = O), 740–880 (M-O-M). ^{1}H NMR (400 MHz, DMSO-d_6) δ (ppm) = 9.1 (s, 1H, NCHN), 7.78 (s, 1H, NCH), 7.72 (s, 1H, NCH), 4.21 (t, J = 7.1 Hz, 2H, NCH_2), 3.89 (s, 3H, NCH_3), 1.81 (m, 2H, CH_2), 1.25 (dq, J = 14.7, 7.3 Hz, 2H, CH_2), 0.85 (t, J = 7.4 Hz, 3H, but-CH_3). $^{13}C\{^{1}H\}$ NMR (101 MHz, DMSO-d_6) δ (ppm) = 136.93, 124.11, 122.76, 56.48, 36.2, 31.84, 19, 13.74. $^{31}P\{^{1}H\}$ NMR (162 MHz, DMSO-d_6) δ (ppm) = −1.44 (minor), −4.61 (major).

$(BuPyr)_5PMo_{10}V_2$: $H_5PMo_{10}V_2O_{40}.31H_2O$ (1 g, 0.43 mmol) was mixed with 1-butylpyridinium bromide (0.47 g, 2.1 mmol) in 10 mL water at room temperature for 4 h. The light orange salt formed was filtered and dried under vacuum. Yield: 92 %. Elem. Anal. Calc: C, 22.30; H, 2.00; N, 2.90. Found: C, 19.60; H, 2.16; N, 2.61. ATR-IR $\nu(cm^{-1})$: 3150–2850 (CH), 1629 (C=C), 1484 (C—N), 1052 (P—O), 942 (Mo = O), 740–880 (Mo-O-Mo). ^{1}H NMR (400 MHz, DMSO-d_6) δ (ppm) = 9.01 (d, J = 5.4 Hz, 2H, Py-CHN), 8.53 (t, J = 7.8 Hz, 1H, Py-CH), 8.10 (t, J = 7.1 Hz, 2H, Py-CH), 4.57 (t, J = 7.4 Hz, 2H, NCH_2), 1.84 (p, J = 7.7 Hz, 2H, CH_2), 1.22 (1.21 (h, J = 7.4 Hz, 2H, CH_2), 0.82 (t, J = 7.4 Hz, 3H, but-CH_3). $^{13}C\{^{1}H\}$ NMR (101 MHz, DMSO-d_6) δ (ppm) = 145.73, 144.96, 128.41, 60.96, 32.97, 19.02, 13.59. $^{31}P\{^{1}H\}$ NMR (162 MHz, DMSO-d_6) δ (ppm) = −4.58.

$(TBA)_3PMo_{12}$: $H_3PMo_{12}O_{40}.21H_2O$ (1 g, 0.45 mmol) was mixed with tetrabutylammonium bromide (0.41 g, 1.3 mmol) in 10 mL water at room temperature for 4 h. The light-yellow salt formed was filtered and dried under vacuum. Yield: 90 %. Elem. Anal. Calc: C, 22.60; H, 4.20.; N, 1.60. Found: C, 22.80; H, 4.31; N, 1.80. ATR-IR $\nu(cm^{-1})$: 3000–2850 (CH), 1060 (P—O), 950 (Mo = O), 873 (C—N), 740–880 (Mo-O-Mo). ^{1}H NMR (400 MHz, DMSO-d_6) δ (ppm) = 3.18 (m, 8H, CH_2N), 1.58 (m, 8H, CH_2), 1.34 (m, 8H, CH_2), 0.95 (t, J = 7.3 Hz, 12H, CH_3). $^{13}C\{^{1}H\}$ NMR (101 MHz, DMSO-d_6) δ (ppm) = 59.97, 23.53, 19.69, 13.97. $^{31}P\{^{1}H\}$ NMR (162 MHz, DMSO-d_6) δ (ppm) = −1.1 (minor), −4.12 (major).

$(TBA)_4PMo_{11}V$: $H_3PMo_{11}VO_{40}.28H_2O$ (1 g, 0.43 mmol) was mixed with tetrabutylammonium bromide (0.54 g, 1.7 mmol) in 10 mL water at room temperature for 4 h. The orange salt formed was filtered and dried under vacuum. Yield: 93 %. Elem. Anal. Calc: C, 27.90; H, 5.20.; N, 2.40. Found: C, 27.23; H, 4.88; N, 2.42. ATR-IR $\nu(cm^{-1})$: 3000–2850 (CH), 1058 (P—O), 952 (Mo = O), 872 (C—N), 740–880 (Mo-O-Mo). ^{1}H NMR (400 MHz, DMSO-d_6) δ (ppm) = 3.17 (m, 8H, CH_2N), 1.57 (m, 8H, CH_2), 1.33 (m, 8H, CH_2), 0.94 (t, J = 7.3 Hz, 12H, CH_3). $^{13}C\{^{1}H\}$ NMR (101 MHz, DMSO-d_6) δ (ppm) = 56.48, 23.53, 18.94, 13.95. $^{31}P\{^{1}H\}$ NMR (162 MHz, DMSO-d_6) δ (ppm) = −4.60.

$(TBA)_5PMo_{10}V_2$: $H_5PMo_{10}V_2O_{40}.31H_2O$ (1 g, 0.43 mmol) was mixed with tetrabutylammonium bromide (0.67 g, 2.1 mmol) in 10 mL water at room temperature for 4 h. The brick orange salt formed was filtered and dried under vacuum. Yield: 95 %. Elem. Anal. Calc: C, 32.60; H, 6.11.; N, 2.30. Found: C, 30.46; H, 5.95; N, 2.26. ATR-IR $\nu(cm^{-1})$: 3000–2850 (CH), 1057 (P—O), 953 (Mo = O), 871 (C—N), 740–880 (Mo-O-Mo). ^{1}H NMR (400 MHz, DMSO-d_6) δ (ppm) = 3.09 (m, 8H, CH_2N), 1.5 (m, 8H, CH_2), 1.25 (m, 8H, CH_2), 0.85 (t, J = 7.3 Hz, 12H, CH_3). $^{13}C\{^{1}H\}$ NMR (101 MHz, DMSO-d_6) δ (ppm) = 57.99, 23.55, 19.67, 13.98. $^{31}P\{^{1}H\}$ NMR (162 MHz, DMSO-d_6) δ (ppm) = −4.38.

2.3.3. Stöber silica synthesis: ***SiO_2*** *[32]*

36 mL of H_2O (2 mol) and 33 mL of ammonia aqueous solution (28 % wt) were mixed in 315 mL (7.8 mol) of methanol at room temperature. Tetraethyl orthosilicate (20 mL, 0.09 mol) is added into the solution and a white solid suspension appeared. The mixture was stirred at 55 °C for 6 h. The solid was washed with absolute ethanol (5 mL) four times and collected by centrifugation. SiO_2 nanoparticles were dried under vacuum at 120 °C overnight. A white powder was obtained. Elem. Anal. Found: C, 1.21 %; H, 0.87 %. ATR-IR $\nu(cm^{-1})$: 2930–3707 (OH), 1053 (Si–O–Si), 942 (Si–OH), 795 and 434 (Si–O–Si). ^{29}Si CP MAS-NMR: δ (ppm) = −92.1 (Q_2), −102.6 (Q_3), −112.5 (Q_4).

2.3.4. General synthesis of SiO_2@Cl, SiO_2@Imd, SiO_2@Pyr and SiO_2@POM

Chloropropyl substituted silica (**SiO_2@Cl**) was prepared by reaction of 3-chloropropyltriethoxysilane with **SiO_2** [41]. **SiO_2@Imd** and

SiO_2@Pyr were synthesized by the substitution of the chlorine with methyl imidazole and pyridine respectively according to reported procedure [42]. The grafting of the POMs on the functionalized silica **SiO_2@Imd** and **SiO_2@Pyr** was realized by refluxing the functionalized silica (1 g) after being sonicated in water, with the corresponding HPAs (0.3 g) in 5 mL H_2O overnight. The obtained product was washed 3 times with water after centrifugation. All the products were dried at 100 °C overnight.

$SiO_{2@Cl}$: ATR-IR $\nu(cm^{-1})$: 2700–3700 (OH), 1440 (CH_2), 1049 (Si–O–Si), 939 (Si–OH), 860 (CH_2-Cl) 785 and 429 (Si–O–Si). ^{29}Si CP MAS-NMR: δ (ppm) = −60.28 (T_2), −68.17 (T_3), −94.21 (Q_2), −102.67 (Q_3) –111.16 (Q_4). ^{13}C CP MAS-NMR δ (ppm) = 58.79, 51.12, 45.11, 26.53, 16.85, 9.90.

$SiO_{2@Imd}$: E.A found (%): C = 2.11, H = 0.86, *N* = 0.49. Imd loading:175 μmol/g. ATR-IR $\nu(cm^{-1})$: 3000–3600 (OH and N—H), 1660 (C=N), 1049 (Si–O–Si), 962 (Si–OH), 795 and 440 (Si–O–Si). ^{29}Si CP MAS-NMR: δ (ppm) = −59.12 (T_2), −68.96 (T_3), −93.78 (Q_2), −102.58 (Q_3), −111.17 (Q_4). ^{13}C CP MAS-NMR: δ (ppm) = 165.16, 137.27, 123.08, 58.86, 51.63, 35.18, 25.3, 17.21, 9.93.

$SiO_{2@Pyr}$: E.A found (%): C = 1.76, H = 0.46, *N* = 0.14. Pyr loading 102 μmol/g. ATR-IR $\nu(cm^{-1})$: 2800–3600 (OH and N—H), 1620 (C=N), 1056 (Si–O–Si), 948 (Si–OH), 796 and 437 (Si–O–Si)·^{29}Si CP MAS-NMR: δ (ppm) = −61.29 (T_2), −69.35 (T_3), −93.78 (Q_2), −102.63 (Q_3), −111.57 (Q_4). ^{13}C CP MAS-NMR: δ (ppm) = 145.35, 137.15, 135, 128.58, 123.2, 61.11, 58.80, 51.58, 35.9, 24.89, 17.21, 9.77.

$SiO_{2@Imd@PMo_{12}}$: ^{29}Si CP MAS-NMR: δ (ppm) = −58.9 (T_2), −68.17 (T_3), −93.78 (Q_2), −102.65 (Q_3), −111.54 (Q_4). ^{13}C CP MAS-NMR δ (ppm) = 136.15, 124.11, 47.53, 36.50, 26.67, 10.6. ^{31}P CP MAS-NMR: δ (ppm) -3.72. IR-ATR, $\nu(cm^{-1})$ for all grafted POMs: 1055–1100 (P—O), 1000–900 (M-O), 850–700 (M-O-M). **PMo_{12}** loading = 37.0 μmol/g.

$SiO_{2@Imd@PMo_{11V}}$: ^{29}Si CP MAS-NMR δ (ppm) = −64.64 (T_3), −93.82 (Q_2), −102.67 (Q_3) –111.58 (Q_4). ^{13}C CP MAS-NMR δ (ppm) = 143.29, 128.34, 62.35, 50.48, 24.19, 15.85, 8.3. ^{31}P CP MAS-NMR δ (ppm) = −4.25. **$PMo_{11}V$** loading = 62.6 μmol/g.

$SiO_{2@Imd@PMo_{10V2}}$: ^{29}Si CP MAS-NMR: δ (ppm) = −68.86 (T_3), −94.00 (Q_2), −102.48 (Q_3), −110.95 (Q_4). ^{13}C CP MAS-NMR δ (ppm) = 135.15, 124.13, 46.43, 36.25, 26.22, 10.7. ^{31}P CP MAS-NMR: δ (ppm) = −4.23. **$PMo_{10}V_2$** Loading = 51.2 μmol/g.

$SiO_{2@Pyr@PMo_{12}}$: ^{29}Si CP MAS-NMR: δ (ppm) = −57.92 (T_2), −69.71 (T_3), −94.09 (Q_2), −102.62 (Q_3), −111.62 (Q_4). ^{13}C CP MAS-NMR: δ (ppm) = 143.29, 128.34, 62.35, 50.48, 24.19, 15.85, 8.3. ^{31}P CP MAS-NMR: δ (ppm) = −3.78. **PMo_{12}** Loading = 30.2 μmol/g.

$SiO_{2@Pyr@PMo_{11V}}$: ^{29}Si CP MAS-NMR: δ (ppm) = −60.3 (T_2), −69.77 (T_3), −93.67 (Q_2), −102.57 (Q_3), −111.37 (Q_4). ^{13}C CP MAS-NMR δ (ppm) = 147.55, 127.33, 72.79, 57.81, 25.13, 16.25, 6.42. ^{31}P CP MAS-NMR: δ (ppm) = −4.08. **$PMo_{11}V$** Loading = 33.3 μmol/g.

$SiO_{2@Pyr@PMo_{10V2}}$: ^{29}Si CP MAS-NMR: δ (ppm) = −57.47 (T_2), −68.96 (T_3), −93.61 (Q_2), −102.87 (Q_3), −111.48 (Q_4). ^{13}C CP MAS-NMR δ (ppm) =146.21, 125.1, 72, 57.77, 24.12, 16.69, 7.13. ^{31}P CP MAS-NMR: δ (ppm) = −4.08. **$PMo_{10}V_2$** Loading = 30.3 μmol/g.

2.4. Catalytic oxidation reactions

In a typical experiment, Linalool **L** (1.54 g, 0.01 mol), dodecane or acetophenone as internal standard (0.1 mL), and 0.0025 equivalents of POMs (as HPAs, in organic salt or grafted) were mixed in a round bottomed flask. According to the nature of oxidant, once the reaction temperature regulated as defined in experimental conditions, 2 equivalents of oxidant (TBHP in water and H_2O_2 in water (with/without additional acetonitrile) were added to start the reaction. The reaction mixture is left under stirring for 5 h in free POMs and organic POMs cases and 24 h in grafted POMs case. Samples of organic phase of the reaction mixture were withdrawn periodically and analyzed by GC-FID.

3. Results and discussion

3.1. Synthesis and characterization of organic salts of POMs

The organic salts of POMs, **OrgPOMs**, were synthesized and evaluated to assess the impact of deprotonation on catalytic performance. **OrgPOMs** were also synthesized to mimic the ionic grafting of POMs onto silica (see infra). These salts combine both POM core's and organic cation's intrinsic properties [29]. Their syntheses were carried out in water at room temperature via a simple mixing procedure involving HPAs ($H_3PMo_{12}O_{40}$, $H_4PMo_{11}V_1O_{40}$ and $H_5PMo_{10}V_2O_{40}$) and onium halide **OrgX** (tetrabutylammonium bromide Bu_4NBr, butylmethylimidazolium chloride BmImCl, or 1-butyl-pyridinium bromide BuPyrBr) using an optimized **OrgX/HPA** molar ratio (Scheme 2). This green, energy-efficient method requires no external thermal energy input. After stirring, the solid products were filtered, dried, and tested for their catalytic activity in the oxidation of linalool. Following this strategy, **$(Org)_3PMo_{12}$**, **$(Org)_4PMo_{11}V$** and **$(Org)_5PMo_{10}V_2$** were obtained and characterized.

While the structure of **$(BuPyr)_3PMo_{12}$** was already reported [29], slow evaporation of a saturated solution of **$(BmIm)_3PMo_{12}$** in a mixture of DMSO/CH_3CN (50/50) afforded green single crystal, suitable for X-ray diffraction analysis. The corresponding solid-state molecular structure is depicted in Fig. 1. As expected, the molecular unit is composed of the well-known Keggin $[PMo_{12}O_{40}]^{3-}$ anion surrounded by three butyl methyl imidazolium cations. All the bonding parameters in the trianion agree with those found in the structure of **$(BuPyr)_3PMo_{12}$**.

3.2. Synthesis and characterization of immobilized POMs

The catalytic objects were synthesized in four steps [43] (Scheme 3). The first one was the synthesis of the non-porous silica beads (**SiO_2**) by condensation of tetraethyl orthosilicate (TEOS) in MeOH according to the Stöber method [44]. The **SiO_2** surface was then functionalized using chloropropyltriethoxysilane in toluene to access to **SiO_2@Cl** [45]. Substitution of the chloride group allowed the introduction of the targeted cationic groups ($BmIm^+$ or $BuPyr^+$) on the surface of silica beads, leading to **SiO_2@Org** materials, respectively **SiO_2@Imd** and **SiO_2@Pyr**, the organic groups mimicking the organic cations used for **OrgPOMs**. The final step was the ionic immobilization of POMs on the surface of **SiO_2@Imd** and **SiO_2@Pyr** by mixing HPAs and **SiO_2@Org** in water, leading to **SiO_2@Org@PM**, the final catalytic objects.

SiO_2@Org@PMo_{12} were isolated as pale green powders whereas **SiO_2@Org@$PMo_{11}V$** and **SiO_2@Org@$PMo_{10}V_2$** were isolated as yellow powders (Org = Imd and Org).

Amorphous nature, as well as sizes and morphologies of isolated objects **SiO_2**, **SiO_2@Cl**, **SiO_2@Org** and **SiO_2@Org@PM** were analyzed before catalytic experiments by PXRD, DLS, EDX, SEM and solid-state NMR. Quantitative studies were performed through elemental analysis and $^{31}P\{^1H\}$ solution NMR. Selected data essential to the catalytic study are discussed in the main manuscript. All additional characterization details are provided in the Supporting Information.

The functionalization of the silica surface with chloropropylsilane was confirmed by multinuclear CP-MAS NMR spectroscopy, which revealed three additional peaks compared to naked silica. These peaks are attributed to the chloropropyl moiety (see Fig. S11 in the Supporting Information). Analysis of nitrogen content indicated that the amounts of grafted Pyr and Imd were 0.102 mmol/g and 0.175 mmol/g of **SiO_2**, respectively (Table 1). The amount of grafted POM was quantified by liquid-state $^{31}P\{^1H\}$ NMR spectroscopy using an external calibration curve prepared with H_3PO_4 solutions at pH 13 (Table 1) [46].

Based on elemental analysis and NMR quantification, the POM/organic ligand molar ratios were calculated for all hybrid materials. For the reactions involving $H_3PMo_{12}O_{40}$, the ratios were 0.296 for **SiO_2@-Pyr@PMo_{12}** and 0.211 for **SiO_2@Imd@PMo_{12}** (Table 1), both lower than the theoretical value of 0.333 if all cations grafted on the silica were

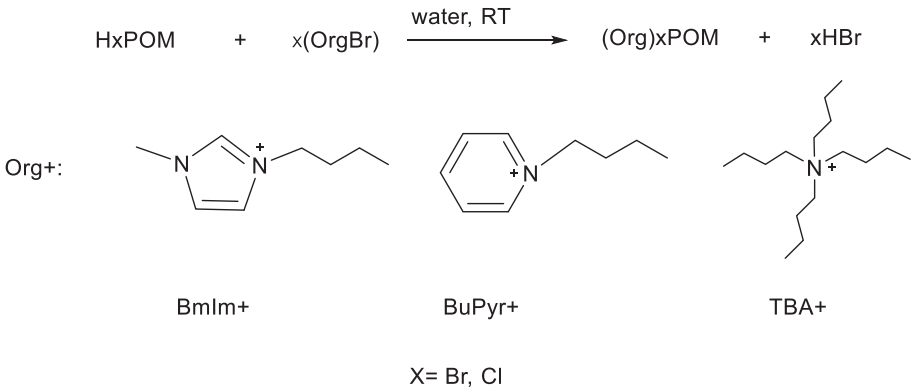

Scheme 2. Organic salts synthesis scheme

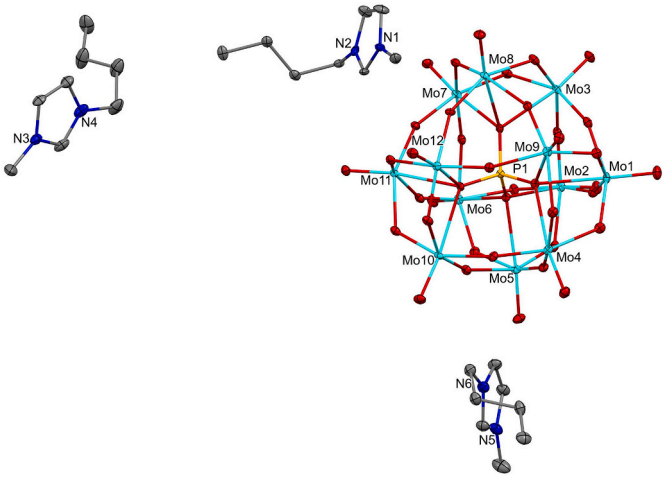

Fig. 1. View of the molecular structure of **$(BmIm)_3PMo_{12}$**. The hydrogen atoms were omitted for clarity. Ellipsoids are represented at the 50 % probability level. Cyan (Molybdenum), Red (oxygen), Orange (Phosphorus), Grey (Carbon) and purple (Nitrogen). (For interpretation of the references to colour in this figure legend, the reader is referred to the web version of this article.)

used to compensate the charge of the POMs (corresponding to a 1:3 POM/ligand ratio). In contrast, with $H_4PMo_{11}VO_{40}$, the experimental ratios were higher: 0.326 for **SiO_2@Pyr@$PMo_{11}V$** and 0.358 for **SiO_2@Imd@$PMo_{11}V$**, while the expected value would be of 0.25. A similar trend was observed for $H_5PMo_{10}V_2O_{40}$, with values of 0.297 (**SiO_2@Pyr@ $PMo_{10}V_2$**) and 0.293 (**SiO_2@Imd@$PMo_{10}V_2$**) versus an expected ratio of 0.20. These higher-than-expected values suggest that the POMs are not fully deprotonated. In some cases, grafting efficiencies exceeding 100 % may result from incomplete coordination of the organic ligands, the interaction of multiple POM units with a limited number of ligands, or possible aggregation of POMs on the surface. Surface coverage was then determined as previously described, yielding values ranging from 0.4 to 0.9 mmol of POM per nm^2 [46]. These values are relatively high for Keggin-type POMs grafted onto Stöber silica, especially when compared to literature data. These obtained POMs loading onto amine-functionalized silica in this study ranged from 0.0303 to 0.0626 mmol/g of silica, this loading being comparable or slightly higher than that reported by Tarlani et al., who achieved 0.0033 mmol/g for $H_3PW_{12}O_{40}$ and 0.071 mmol/g for $H_{15}P_5W_{30}O_{110}$ using a simpler amine-functionalized silica system [31]. It seems that the non-porous nature of Stöber silica allows a more uniform and dense distribution of POMs on the external surface, with strong interactions between the POMs and the functionalized silica surface [47]. From a catalytic perspective, this dense and stable immobilization is particularly promising, potentially enhancing performance in applications such as acid catalysis and redox reactions [48].

Dynamic Light Scattering (DLS) measurements of the **SiO_2**-based samples revealed significant changes in particle size distribution depending on surface modifications. DLS measurements of the **SiO_2** particles yielded a stable hydrodynamic diameter around 190 nm, consistent with monodisperse, non-aggregated particles in aqueous suspension. Upon grafting of the POMs, a significant increase in the hydrodynamic size was observed, with values ranging between 500 and 750 nm depending on the sample, indicating a change of behavior of the silica beads after the grafting of polyoxometalates (POMs) onto the Stöber silica surface (Fig. S31 in the Supporting Information). This size increase can be attributed to several factors: slight aggregation of silica particles induced by the grafting process, and enhanced interparticle interactions due to the presence of functional groups as reported by previous reports, such as the study by Khutoryanskiy et al. where such a phenomenon was observed with thiolated silica particles [49]. **In SEM, the slight increase observed is in accordance with the small modifications of the surface of the beads size distributions were also observed by SEM**. (Fig. S40). These findings complement the molar ratio and surface coverage data, **Furthermore, EDX spectra (Figs. S32–38) confirmed the presence of Cl, N, and POM elements at the various stages of grafting**, reinforcing the conclusions drawn from the structural and compositional analyses.

3.3. Catalyzed oxidation of linalool

As stated in the introduction, a direct access to furanoid (**F**) and pyranoid (**P**) directly for the primary oxidation of linalool (**L**) is particularly interesting for different aspects.

The oxidation of **L** using different synthetized catalysts (HPAs, **OrgPOMs** and **SiO_2@Org@POMs**) was realized as followed (Scheme 4). In all cases, the same quantity of POMs (0.0025 eq) was used. Two oxidants were evaluated, $TBHP_{aq}$ at 80 °C and H_2O_{2aq} at 70 °C. In order to fix some solubilities issues, the use of acetonitrile (ACN) as co-solvent had to be studied, only when H_2O_{2aq} is used as oxidant. Reaction time was 5 h under homogeneous conditions (with HPAs and **OrgPOMs**) and 24 h under heterogenous conditions (with **SiO_2@Org@POMs**). Catalytic reactions were followed by GC-FID using dodecane as internal standard. All reactions were replicated 3 times and consistent results were observed.

As previously reported, the oxidation of linalool leads to the formation of **F** and **P** compounds through an intermolecular cyclization mechanism, as well as a di-epoxide [25,50]. In the present study, only the formation of **F** and **P** was considered. Although the di-epoxide was detected by GC–MS, it was not quantified due to its instability and the fact that it is not commercially available.

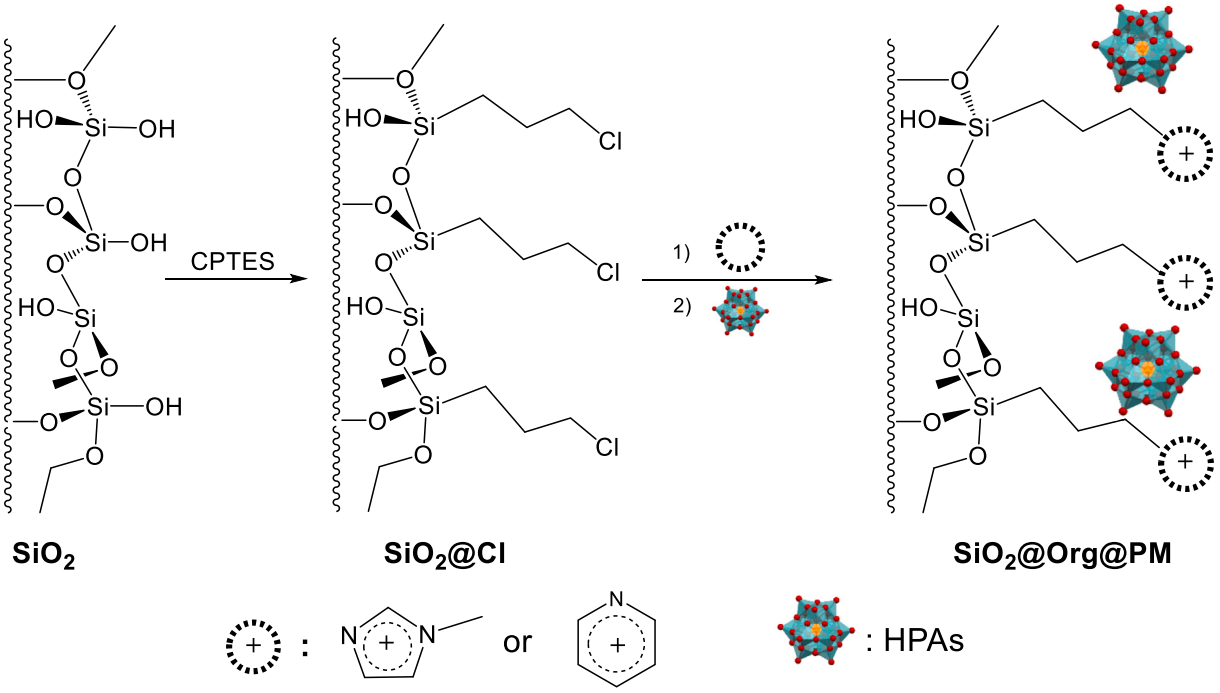

Scheme 3. Synthetic pathway of silica particles

Table 1
Quantitative loading analysis.

Pyr *		POM **	Molar Ratio (x)	POM Surface Coverage (μ)
	SiO_2@Pyr@PMo_{12}	0.0302	0.296	0.473
0.102	**SiO_2@Pyr@$PMo_{11}V$**	0.0333	0.3264	0.522
	SiO_2@Pyr@$PMo_{10}V_2$	0.0303	0.297	0.474
Imd*				
	SiO_2@Imd@PMo_{12}	0.037	0.2114	0.581
0.175	**SiO_2@Imd@$PMo_{11}V$**	0.0626	0.3577	0.981
	SiO_2@Imd@$PMo_{10}V_2$	0.0512	0.2925	0.803

* from E.A with Org: Pyr or Imd (mmol/ 1 g of SiO2),
** from $^{31}P\{^1H\}$ solution NMR (mmol/ 1 g SiO_2). x = nPOM/nOrg, and μ in mmol/nm^2.

3.3.1. *Catalyzed oxidation with HPAs*

The catalytic results obtained with HPAs are summarized in Table 2. All catalysts exhibited high **L** conversions (≥ 85 %), with almost completion when aqueous TBHP was used as oxidant (Entries P1, P4, and P7). The choice of oxidant had a significant impact on the selectivity of oxidation products. The highest **F** + **P** yields were obtained with H_2O_2aq as oxidant and acetonitrile as solvent (Entries P3, P6 and P9), particularly with $H_4PMo_{11}V$ (80 %) (Entry P6) and $H_5PMo_{10}V_2$ (78 %) (Entry P9). $TBHP_{aq}$, on the other hand, lead to significantly lower **F** + **P** yields (2–8 %), indicating that distinct reaction pathways are favored. However, when H_2O_{2aq} was used without solvent, low **F** + **P** yields were obtained (3–8 %) with all the catalysts (Entries P2, P5 and P8). This demonstrates how effectively solvent influences both **F** and **P** formation and favors in this case the selective formation of the targeted products. It is also important to note that the selectivity favors **F** over **P** in all cases. **F** is the kinetic product, formed more rapidly, while **P** is likely the thermodynamic product, more stable but requiring longer times to be formed [25]. Same behavior was observed in the case of $TBHP_{aq}$. Low **F** and **P** yields can be explained by over oxidation and the di-epoxide formation and same preference of **F** over **P**.

3.3.2. *Catalyzed oxidation with organic salts of POMs*

As stated in the introduction part, the goal was to access to POMs immobilized on silica surface by interaction between POMs and cationic functions (pyridinium or imidazolium) present on silica surface. In order to investigate the effect of the cationic moiety on POMs, notably the effect of the acidity, the catalytic activities of **OrgPOMs**, based on the replacement of protons of HAPs by organic cationic parts, butylpyridinium (BuPyr), tetrabutylammonium (TBA) and butylmethylimidazolium (BmIm), have been evaluated under the same conditions as for HPAs. The results of linalool oxidation with the three salts are collected

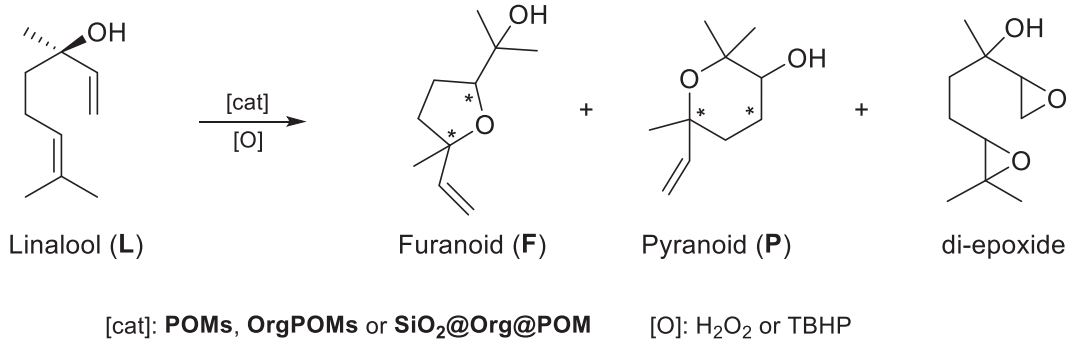

Scheme 4. Linalool Oxidation

Table 2
Linalool Oxidation results using HPAs.

Entry	Catalyst	Oxidant	**L** conv /%	**F** yield /%	**P** yield /%	TON[a]	TOF_{max} [b] /h^{-1}
P1		$TBHP_{aq}$	>99	6	2	394	1182
P2	H_3PMo_{12}	H_2O_{2aq}	98	8	4	332	996
P3		$H_2O_{2\ aq}$ + ACN	85	29	13	338	1014
P4		TBHPaq	>99	2	2	399	1198
P5	$H_4PMo_{11}V$	H_2O_2aq	97	5	2	388	1165
P6		H_2O_{2aq} + ACN	99	49	31	396	1190
P7		$TBHP_{aq}$	>99	1	1	400	1199
P8	$H_5PMo_{10}V_2$	H_2O_{2aq}	97	3	1	389	1167
P9		H_2O_{2aq} + ACN	95	47	31	384	1153

Catalytic conditions: cat/sub/ox molar ratio: 0.25/100/200, 80 °C with $TBHP_{aq}$ and 70 °C with H_2O_{2aq} for 5h. (a) TON = (mol **L** converted /mol catalyst) at 5h (b) TOF_{max} (at 20 min) = mol **L** converted/(mol catalyst × 0.33).

in Tables 3, 4 and 5.

3.3.2.1. Results with butyl pyridinium salts of POMs. When aqueous TBHP was used as oxidant, moderate **L** conversions and low yields of **F** and **P** were observed (Entries Bu1, Bu4, and Bu7). For example, with **$(BuPyr)_3PMo_{12}$** (Entry Bu1), the conversion reached 53 %, but **F** and **P** yields of remained low (5 % and 2 %, respectively). This limited performance can be attributed to the steric hindrance and bulkiness of the butylpyridinium, which likely interfere with the coordination and activation of the peroxide, as well as with electrostatic interactions.

In contrast, use of aqueous H_2O_2 in water led to improved **L** conversions and higher **F** and **P** yields (Entries Bu2, Bu5, and Bu8). For instance, with **$(BuPyr)_3PMo_{12}$** (Entry Bu2), a conversion of 64 % was achieved, along with **F** and **P** yields of 15 % and 11 %, respectively, and a moderate turnover frequency (TOF) of 116 h^{-1}. These results confirm that H_2O_{2aq} is a more effective oxidant under these conditions.

Notably, the addition of acetonitrile as solvent enhanced the reaction efficiency (Entries Bu3, Bu6, and Bu9). Under these conditions, **L** conversions reached up to 98 %, and product yields were significantly improved. The performance observed with all **$(BuPyr)_xPOMs$** (Entries Bu3, Bu6 and Bu9), delivered total **F** + **P** yields of 80, 82 and 78 % respectively.

3.3.2.2. Results with tetrabutylammonium salts of POMs. Similar results were obtained with TBA salts. The lowest **L** conversions and correspondingly low **F** and **P** yields were recorded with $TBHP_{aq}$ as oxidant (Entries T1, T4, and T7). A clear improvement was observed with H_2O_{2aq}, which led to increased **L** conversions and higher **F** + **P** yields (24–51 %) compared to $TBHP_{aq}$. As observed with butylpyridinium salts, the best catalytic performances were achieved using aqueous H_2O_2 as the oxidant and acetonitrile as co-solvent, with 74–98 % of **L** conversion but most importantly 63–76 % of **F** + **P** yields.

3.3.2.3. Results with butylmethylimidazolium salts of POMs. In the case of butylmethylimidazolium (BmIm) salts, similar trends were observed in terms of **L** conversion and **F** and **P** yields. Notably, with **$(BmIm)_3PMo_{12}$** and $TBHP_{aq}$ (Entry Bm1), higher yields of **F** + **P** (44 %) were obtained compared to those achieved with the other organic salts under similar conditions, for example, a maximum of 27 % with **$(BuPyr)_3PMo_{12}$** (Entry Bu4). The best performance was again observed with H_2O_2aq as the oxidant and acetonitrile as co-solvent with **F** + **P** yields in 65–75 % range (entries Bm3, Bm6 and Bm9).

3.3.2.4. General comparison. In comparison to HPAs, **OrgPOMs** generally showed enhanced efficiency, yielding higher yields of **F** + **P** products when using either TBHP or aqueous H_2O_2. Particularly, the use of acetonitrile as solvent with H_2O_2 resulted in the best outcomes in terms of **L** conversion and product yields. Even under solvent-free conditions, organic salts outperformed **HPAs** in terms of **F** and **P** yields. However, despite these advantages, **HPAs** consistently exhibited higher turnover frequencies (TOFs), indicating that POMs are kinetically more active in their acidic form, but with more tendency towards overoxidation. Overall, **HPAs** demonstrated greater catalytic activity and faster reaction rates but lower selectivity towards **F** and **P** likely due to their strong acidity. In contrast, the reactivity of organic salts of POM is highly dependent on both structure of the POM and characteristics of the organic cation. Factors such as organic moiety's ability to stabilize intermediates, to facilitate substrate binding, to modify redox behavior, and to improve solubility might play a role in influencing reaction pathways and selectivity.

Moreover, addition of ACN as co-solvent significantly enhanced **L** conversion and **F** and **P** formation in the case of HPAs and organic salts systems. This improvement observed in all reaction using ACN is likely due to several reasons, increased solubility, a better homogenization of the reaction mixture and a better stabilization of several parts in the process, whether polar transition states, whether reactive intermediates (LO) so that the **P** and **F** products can be formed preferentially and not diepoxide.

It has to be mentioned that, among all the POMs, all organic salts with **$PMo_{10}V_2$** cores are very fast with TOFs around 1080 h^{-1}. This represents the best performance among all three tested POMs.

Table 3
Linalool Oxidation results using butyl pyridinium salts of POMs.

Entry	Catalyst	Oxidant	**L** conv /%	**F** yield /%	**P** yield /%	TON[a]	TOF^b_{max}/h^{-1}
Bu1		$TBHP_{aq}$	53	5	2	213	555
Bu2	**$(BuPyr)_3PMo_{12}$**	H_2O_{2aq}	64	21	19	256	116
Bu3		$H_2O_{2\ aq}$ + ACN	98	50	30	386	793
Bu4		$TBHP_{aq}$	34	18	9	133	101
Bu5	**$(BuPyr)_4PMo_{11}V_1$**	H_2O_{2aq}	55	15	11	222	188
Bu6		H_2O_{2aq} + ACN	98	52	30	394	766
Bu7		$TBHP_{aq}$	29	9	3	118	354
Bu8	**$(BuPyr)_5PMo_{10}V_2$**	H_2O_{2aq}	47	29	16	191	252
Bu9		H_2O_{2aq} + ACN	86	46	32	345	1101

Catalytic conditions: cat/sub/ox molar ratio: 0.25/100/200, 80 °C with $TBHP_{aq}$ and 70 °C with H_2O_{2aq} for 5h. (a) TON = (mol **L** converted /mol catalyst) at 5h (b) TOF_{max} (at 20 min) = mol **L** converted/(mol catalyst × 0.33)

Table 4
Linalool Oxidation results using tetra butyl ammonium salts of POMs.

Entry	Catalyst	Oxidant	**L** conv /%	**F** yield /%	**P** yield /%	TON[a]	TOF^{b}_{max} /h^{-1}
T1		$TBHP_{aq}$	45	6	3	184	424
T2	**$(TBA)_3PMo_{12}$**	H_2O_{2aq}	70	19	16	283	50
T3		$H_2O_{2\ aq}$ + ACN	74	40	23	291	790
T4		$TBHP_{aq}$	22	11	3	93	114
T5	**$(TBA)_4PMo_{11}V$**	H_2O_{2aq}	33	14	10	130	317
T6		H_2O_{2aq} + ACN	98	44	28	391	649
T7		$TBHP_{aq}$	35	10	6	146	53
T8	**$(TBA)_5PMo_{10}V_2$**	H_2O_{2aq}	56	28	23	231	550
T9		H_2O_{2aq} + ACN	87	46	30	352	1061

Catalytic conditions: cat/sub/ox molar ratio: 0.25/100/200, 80 °C with $TBHP_{aq}$ and 70 °C with H_2O_{2aq} for 5h. (a) TON = (mol **L** converted /mol catalyst) at 5h (b) TOF_{max} (at 20 min) = mol **L** converted/(mol catalyst × 0.33).

Table 5
Linalool Oxidation results using butyl methyl imidazolium salts of POMs.

Entry	Catalyst	Oxidant	**L** conv /%	**F** yield /%	**P** yield /%	TON[a]	TOF^{b}_{max} /h^{-1}
Bm1		$TBHP_{aq}$	48	29	15	193	71
Bm2	**$(BmIm)_3PMo_{12}$**	H_2O_{2aq}	76	32	25	299	94
Bm3		$H_2O_{2\ aq}$ + ACN	99	43	32	398	788
Bm4		$TBHP_{aq}$	80	5	3	322	808
Bm5	**$(BmIm)_4PMo_{11}V$**	H_2O_{2aq}	86	49	29	347	132
Bm6		H_2O_{2aq} + ACN	98	44	27	395	804
Bm7		$TBHP_{aq}$	49	5	3	350	881
Bm8	**$(BmIm)_5PMo_{10}V_2$**	H_2O_{2aq}	67	15	9	266	639
Bm9		H_2O_{2aq} + ACN	87	44	31	347	1077

Catalytic conditions: cat/sub/ox molar ratio: 0.25/100/200, 80 °C with TBHPaq and 70 °C with H2O2aq for 5h. (a) TON = (mol L converted /mol catalyst) at 5h (b) TOFmax (at 20 min) = mol L converted/(mol catalyst × 0.33).

3.3.3. Catalyzed oxidation with POMs grafted on silica support

As shown in the previous section, **L** conversions up to 98 % and good **F** and **P** yields were obtained in homogeneous conditions, notably with **OrgPOMs**. Once supported on silica, **SiO_2@Org@POMs** (**Org** being similar environment than molecular objects), have been evaluated herein for the oxidation of **L** with the main objectives to work under solvent-free conditions and to recover and reuse the catalyst. In comparison to homogeneous conditions, reaction time was extended to 24 h to allow completion of the reaction. The catalytic results obtained with **SiO_2@Org@POMs** (Org = Pyr of Imd) are summarized in Table 6.

Both **SiO_2@Imd@POMs** and **SiO_2@Pyr@POMs** have shown promising results in such heterogeneous solvent-free transformations with both $TBHP_{aq}$ and H_2O_{2aq} oxidants. It was proven that the presence of the POMs was necessary for the reaction, since very low **L** conversions (33 and 28 %) were obtained with POM-free silica **SiO_2@Imd** and **SiO_2@Pyr** respectively with $TBHP_{aq}$ as oxidant without detectable **F** and **P** formation (Entries Si01 and Si02).

Table 6
Linalool Oxidation results using **SiO_2@Imd@PM.**

Entry	Catalyst	Oxidant	**L** conv /%	**F** yield /%	**P** yield /%
Si01	**SiO_2@Imd**	$TBHP_{aq}$	33	–	–
Si02	**SiO_2@Pyr**	$TBHP_{aq}$	28	–	–
Si1	**SiO_2@Imd@PMo_{12}**	$TBHP_{aq}$	99	30	32
Si2		H_2O_{2aq}	98	24	21
Si3	**SiO_2@Imd@$PMo_{11}V$**	$TBHP_{aq}$	99	22	6
Si4		H_2O_{2aq}	96	25	29
Si5	**SiO_2@Imd@$PMo_{10}V_2$**	$TBHP_{aq}$	99	16	43
Si6		H_2O_{2aq}	88	31	30
Si7	**SiO_2@Pyr@PMo_{12}**	$TBHP_{aq}$	90	31	26
Si8		H_2O_{2aq}	99	31	31
Si9	**SiO_2@Pyr@$PMo_{11}V$**	$TBHP_{aq}$	99	35	32
Si10		H_2O_{2aq}	93	24	19
Si11	**SiO_2@Pyr@$PMo_{10}V_2$**	$TBHP_{aq}$	99	22	19
Si12		H_2O_{2aq}	92	23	17

For grafted POMs: Exact mass of **SiO_2@Imd@PM** was used in which PM/sub/ox mol ratio: 0.25/100/200, T=80 °C with $TBHP_{aq}$ and T=70 °C with H_2O_{2aq} for 5h/

In the case of **SiO_2@Imd@POMs**, the catalysts exhibit high conversion rates, almost full completion with $TBHP_{aq}$ (Entries Si1, Si3, Si5). Among these, **SiO_2@Imd@PMo_{12}** stands out with a balanced production, yielding 62 % of **F** + **P**, with quite balanced **F**/**P** ratio (Entry Si1). **SiO_2@Imd@$PMo_{11}V$** (Entry Si4) and **SiO_2@Imd@$PMo_{10}V_2$** (Entry Si6) produced a **F** + **P** yield of 28 % and 59 % respectively, both with favorable selectivity for **P**, which may warrant further investigation or optimization. When switching to H_2O_{2aq}, very high to full **L** conversion was also obtained (Entries Si2, Si4 and Si6), with high yields (54–61 %) and quite identical **F** and **P** quantities, indicating that the choice of oxidant (and also the functionalization of silica, Imd in this case) seems to influence the product distribution. Different performance of the same POM was obtained with different oxidants. However, no general trend can be determined and results seems to be catalyst dependent.**SiO_2@Pyr@POM** systems present similar conversion efficiencies, with catalysts achieving high conversion rates and noteworthy yields. In all cases, very high **L** conversion was obtained, with a competitive amount of **F** and **P**. Among the $TBHP_{aq}$ entries, **SiO_2@Pyr@PMo_{12}** achieved a 90 % **L** conversion with **F** + **P** yield of 57 % (Entry Si7) with balanced **F**/**P** ratio and **SiO_2@Pyr@$PMo_{11}V$** gave full conversion and 67 % **F** + **P** yield (Entry Si9). This example is one of the most productive systems overall. This suggested that the incorporation of vanadium into the POM structure, enhanced the catalyst's dual selectivity and overall activity.

When comparing the imidazolium-based **SiO_2@Imd@POMs** and pyridinium-based **SiO_2@Pyr@POMs** systems, both exhibited excellent catalytic performance under solvent-free conditions, achieving near-complete linalool conversions with either $TBHP_{aq}$ or H_2O_{2aq}. However, subtle differences in selectivity and product distribution emerge. Imidazolium-functionalized catalysts generally presented more variable selectivity, with some systems favoring **F** or **P** more distinctly depending on the POM composition, whereas pyridinium-based catalysts tended to provide more balanced **F** and **P** yields across different oxidants. This may

be attributed to differences in steric bulk, electronic properties, or the nature of interaction between the organic moiety and the POM, affecting substrate orientation and intermediate stabilization on the catalyst surface.

Regarding the oxidants, both $TBHP_{aq}$ and H_2O_{2aq} enable high conversions, but they differed in their influence on product selectivity. TBHP tended to produce sharper selectivity profiles, often favoring either **F** or **P** more prominently depending on the catalyst, while H_2O_2 typically led to more balanced **F** and **P** yields. These trends suggested that TBHP may drive faster kinetically controlled pathways, while H_2O_2 allowed more thermodynamic equilibration and broader access to both product types, and its ability to produce both products makes it a useful option for certain applications, especially when milder reaction conditions or environmental considerations are prioritized since it forms water as a byproduct.

Since the performance of the catalysts varied significantly, no fixed trends could be established. Different behaviors were observed when altering the catalyst, using the same catalyst with different oxidants, or employing the same oxidant with various organic linker groups attached to the silica. However, it has been shown that organic forms exhibited more efficient and distinct performance across different polyoxometalates (POMs). The primary focus of this study was to achieve the most environmentally sustainable approach possible through catalyst grafting. This method has yielded promising results in terms of conversion rates and product yields, which were often superior to those observed in homogeneous catalysis, even in the presence of solvents.

3.3.4. *Catalyst recyclability*

Considering the activity and selectivity of these supported POMs systems, their practical value also hinges on recyclability and stability. Therefore, the reusability of selected **SiO_2@Org@POM**s catalysts was evaluated under optimized conditions to assess performance retention across multiple cycles and determine their suitability for sustainable, heterogeneous oxidation processes. The results are shown in Figs. 2 and 3.

According to the results, consistent catalytic performance was observed across four consecutive experimental runs in most cases. After each run, the **SiO_2@Org@POM** catalysts were filtered, washed several times, dried, and reused. The catalysts maintained high conversion rates and similar selectivity towards the desired products throughout the tests, with only minimal variations. However, in the case of pyridinium-based systems, a slight decrease in **L** conversion was observed after each cycle. This decline was particularly pronounced with **SiO_2@Imd@P-$Mo_{10}V_2$** when $TBHP_{aq}$ was used as the oxidant (Fig. 2), where significant degradation of the POM structure was confirmed by ^{31}P CP MAS NMR (Fig. 4). This degradation led to low **F** and **P** yields.

The degradation of POMs grafted onto silica, particularly after catalysis, is a plausible explanation for the changes observed in the ^{31}P MAS NMR spectra (Fig. 4). These changes include a decrease in the intensity of the main peak and the appearance of a secondary peak when comparing the fresh catalyst with the same material after four consecutive catalytic cycles. This degradation refers to the structural breakdown or alteration of the POM framework, which may result from chemical, thermal, or mechanical stress during catalysis. The presence of water in the reaction medium appears to play a key role in this process. This is supported by the fact that more pronounced decomposition was observed when using H_2O_2as the oxidant, since it generates water as a byproduct, compared to TBHP, which does not release water upon activation.

Strong interactions between H_2O_2 and POMs are known to occur, especially during redox reactions. POMs can catalyze the synthesis of peroxo species (M-O-O) on the metal centers (M = Mo or W) that results in the disproportionation of H_2O_2 into water and oxygen [27,51]. Because of their high reactivity, these peroxo species can occasionally cause the POM framework to be destroyed and leads to over-oxidation. With TBHP, the reaction mechanism is different. The *tert*-butyl group in TBHP makes it less reactive towards POMs in this way [52]. Such interactions, **partial decomposition** or **fragmentation** of the POM structure might lead to the formation of new phosphorus species, reflected in the additional small peak.

Overall, the supported **SiO_2@Org@POM** catalysts demonstrated good stability and robustness over four consecutive reaction cycles. Although a gradual decrease in linalool conversion was observed, the overall activity remained comparable and competitive. Importantly, the

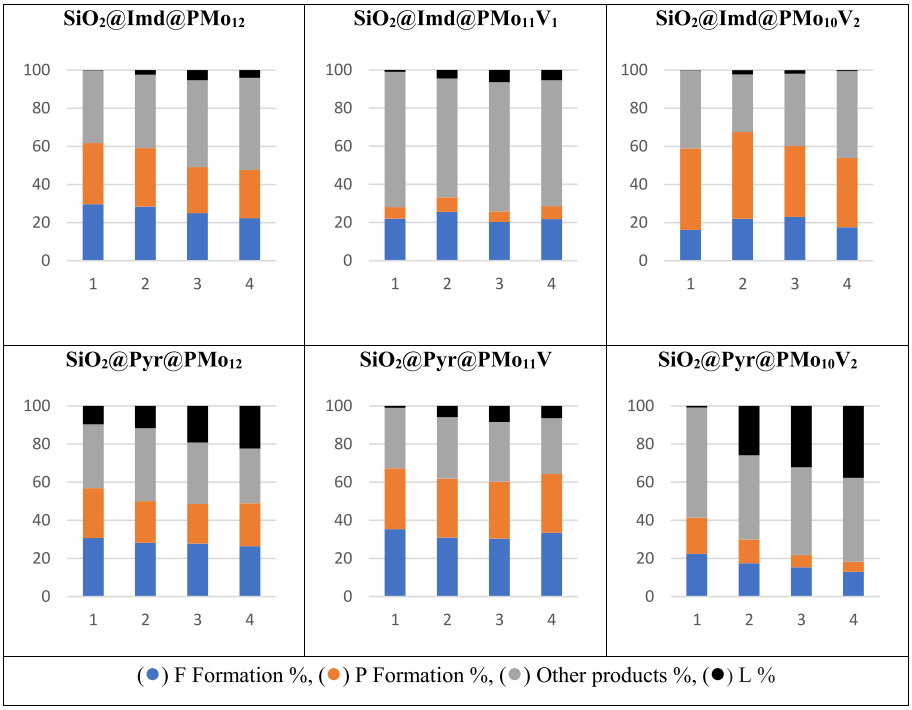

Fig. 2. Catalytic Performance of **SiO_2@org@POMs** systems using TBHP as oxidant up to four runs.

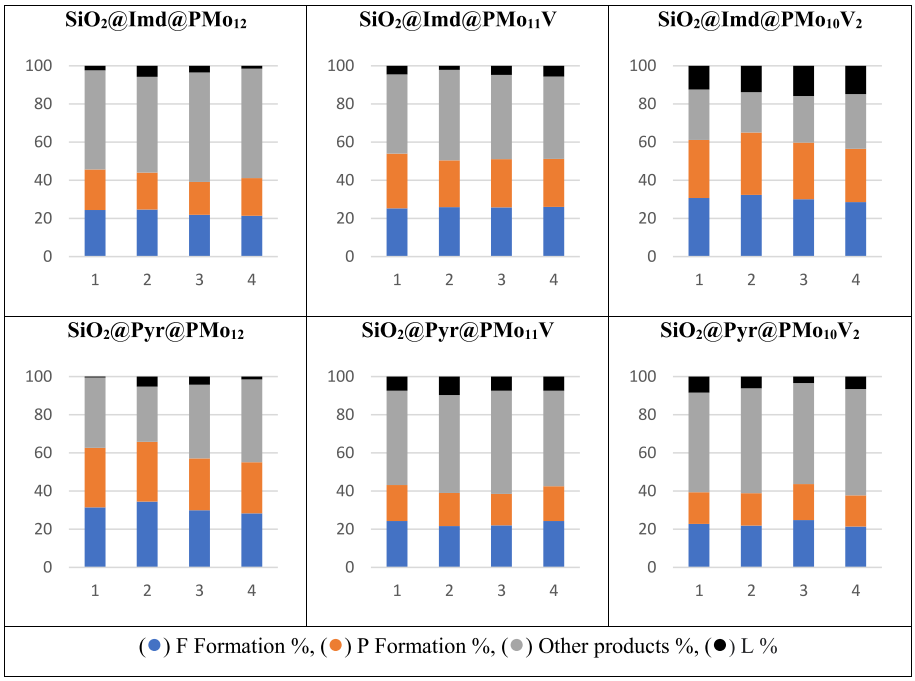

Fig. 3. Catalytic Performance of **SiO_2@Org@POMs** systems using H_2O_{2aq} as oxidant up to four runs.

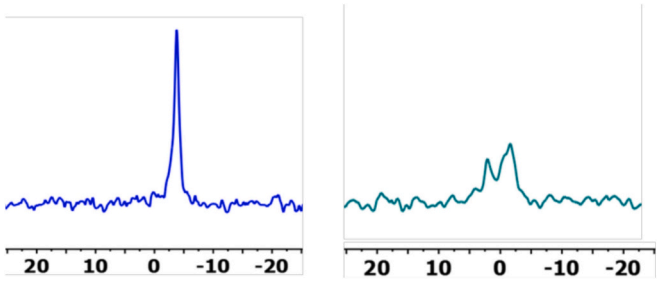

Fig. 4. ^{31}P MAS NMR Spectra of **SiO_2@Pyr@PMo_{12}** before catalysis (left) and after 4th run (right) with $TBHP_{aq}$.

catalysts continued to exhibit meaningful selectivity towards the desired **F** and **P** products, maintaining their dual-product capability. This performance under reuse conditions highlights the structural resilience of the hybrid systems and reinforces their suitability for greener, more sustainable oxidation processes. Compared to their homogeneous counterparts, these heterogeneous catalysts offer clear advantages in terms of recoverability, operational simplicity, and long-term efficiency without compromising product distribution or reaction effectiveness.

3.4. Green metrics considerations

The examples provided (Fig. 5) illustrate several key aspects related to both sustainability and catalytic efficiency, which are consistently reflected across most of the results. All green metrics charts for all the reactions, as well as the specific considerations (formula and conditions) for those metrics are listed in SI. [53]

First, the use of **OrgPOMs**, such as **$(BmIm)_3PMo_{12}$** and **$(BuPyr)_4PMo_{11}V$**, has significantly improved the selectivity of oxidation reaction. These salts enable better reactivity towards the aimed products over the reaction, leading higher yields and enhanced selectivity compared to their parent POMs. This improvement is particularly notable with H_2O_2, as the reaction is more efficient and the process greener due to the benign byproduct (water). Even though it still gave better results with TBHP which can be seen in **$(BmIm)_3PMo_{12}$** and in many other cases as seen above. However, according to the charts, TBHP-based reactions are less favorable compared to H_2O_2 due to the generation of *tert*-butanol as a waste product, further reducing the green chemistry metrics like AE.

Second, the comparison between H_2O_2in water and TBHP in water versus the use of H_2O_2in water with acetonitrile (ACN) demonstrates that both $H_2O_2$and TBHP on their own are more environmentally friendly than the ACN-based system. The addition of ACN not only introduces a solvent, detrimental to the green profile of the process, but also lowers the overall reaction mass efficiency (RME) and atomic economy (AE), even if better yields were obtained as shown in the charts. Both H_2O_2 and TBHP in water produce better results because they avoid the use of additional solvents, with H_2O_2 being the superior oxidant due to its clean byproduct, water, while TBHP generates *tert*-butanol, which is less desirable in terms of waste management.

Lastly, grafting POMs onto silica, such as in **SiO_2@Imd@PMo_{12}** and **SiO_2@Pyr@$PMo_{11}V$**, has proven to be the most sustainable and efficient approach for this oxidation process. This method not only validates the solvent-free protocol which eliminates the need for organic solvents entirely, but also offers the advantage of catalyst recovery, ensuring that the catalyst is not wasted and can be reused multiple times. The grafted POM systems using H_2O_2 in water result in the highest AE, RME, and yield, while producing the least waste, making it the greenest process for the oxidation of linalool. By combining solvent-free conditions with the recyclability of the catalyst and the use of H_2O_2 as the oxidant, the silica-grafted POMs present the optimal pathway for maximizing both efficiency and sustainability in this reaction.

4. Conclusion

In this study, the oxidation of linalool, a natural substrate, was successfully carried out to produce two important structural scaffolds, **furanoid** and **pyranoid** derivatives. Using heteropoly acids (HPAs) and organic salts of polyoxometalates (POMs), a homogeneous catalytic system was developed, demonstrating high efficiency and better activity for the V-containing POMs or when supported on silica. To further enhance the sustainability of the process, functionalized silica was employed for heterogeneous catalysis, enabling the use of a **solvent-**

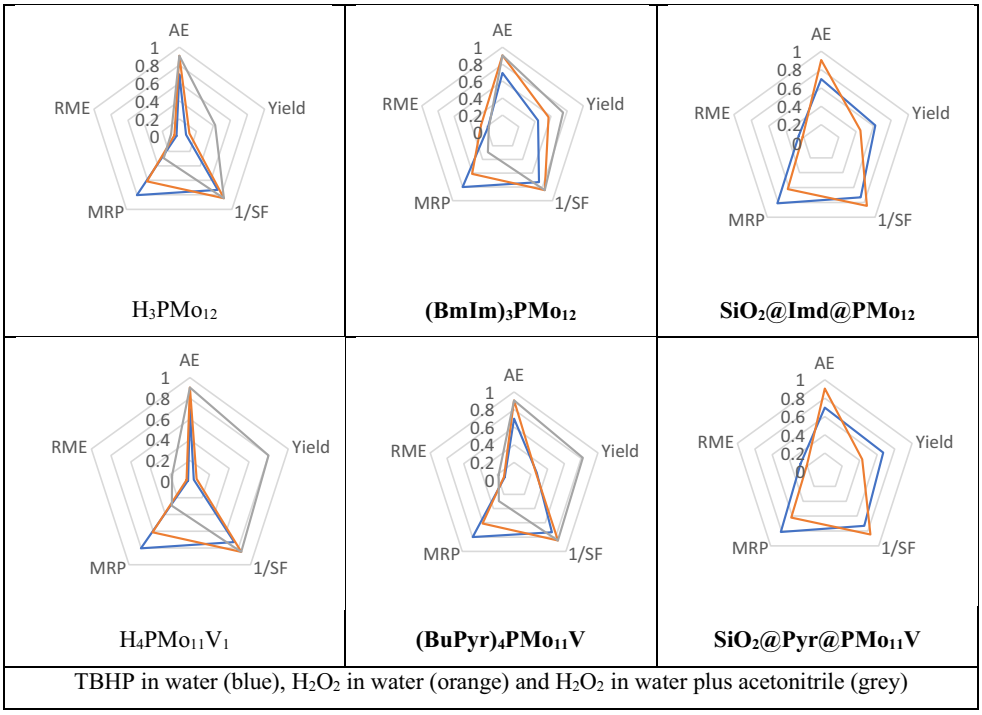

Fig. 5. Radial distribution with Green metrics for two different examples in acidic, organic and grafted forms. TBHP as oxidant in blue, H_2O_2aq in orange, and, H_2O_2aq with CH_3CN solvent in grey. (For interpretation of the references to colour in this figure legend, the reader is referred to the web version of this article.)

free protocol. With most of the catalytic systems, this approach not only maintained excellent conversion rates and selectivity but also allowed for the recovery and reuse of the catalytic system for up to **four cycles** without significant loss of activity. These results are significant from a **green chemistry** perspective, showcasing an efficient, recyclable, and environmentally friendly method for synthesizing valuable chemical scaffolds from renewable resources, opening the field to process intensification through continuous-flow techniques.

CRediT authorship contribution statement

Ali Al Hadi Haidar: Writing – review & editing, Writing – original draft, Validation, Methodology, Investigation, Formal analysis. **Sonia Mallet-Ladeira:** Writing – review & editing, Investigation, Formal analysis, Data curation. **Pascal Guillo:** Writing – review & editing, Writing – original draft, Validation, Supervision, Project administration, Methodology, Funding acquisition, Formal analysis, Data curation, Conceptualization. **Dominique Agustin:** Writing – review & editing, Writing – original draft, Validation, Supervision, Resources, Project administration, Methodology, Funding acquisition, Formal analysis, Data curation, Conceptualization.

Funding

This work was funded by the CNRS, the Région Occitanie [Project GreenCatNat grant number N° 00138053/22009739], the IUT Toulouse Auch Castres and the IUT Chemistry Department and the Syndicat Mixte de la Communauté d'Agglomération Castres-Mazamet.

Declaration of competing interest

The authors declare that they have no known competing financial interests or personal relationships that could have appeared to influence the work reported in this paper.

Acknowledgments

Authors wish to acknowledge the CNRS and the IUT for the facilities. Dr. Yannick Coppel and Dr. Vincent Collière are warmly acknowledged.

Appendix A. Supplementary data

Supplementary data to this article can be found online at https://doi.org/10.1016/j.apcato.2025.207074.

Data availability

Data will be made available on request.

References

[1] E.T. Poursaitidis, P.L. Gkizis, I. Triandafillidi, C.G. Kokotos, Organocatalytic activation of hydrogen peroxide: towards green and sustainable oxidations, Chem. Sci. 15 (2024) 1177–1203, https://doi.org/10.1039/D3SC05618J.
[2] Z. Wei, S. Ru, Q. Zhao, H. Yu, G. Zhang, Y. Wei, Highly efficient and practical aerobic oxidation of alcohols by inorganic-ligand supported copper catalysis, Green Chem. 21 (2019) 4069–4075, https://doi.org/10.1039/C9GC01248F.
[3] H. Kwart, J.H. Nickle, Transition states in chromium(VI) oxidation of alcohols, J. Am. Chem. Soc. 95 (1973) 3394–3396, https://doi.org/10.1021/ja00791a059.
[4] M. Rahman, J. Rocek, Chromium(IV) oxidation of primary and secondary alcohols, J. Am. Chem. Soc. 93 (1971) 5455–5462, https://doi.org/10.1021/ja00750a024.
[5] W.L. Evans, J.E. Day, The oxidation of ethyl alcohol by means of potassium permanganate, J. Am. Chem. Soc. 41 (1919) 1267–1285, https://doi.org/10.1021/ja02229a014.
[6] A. Jordan, P. Stoy, H.F. Sneddon, Chlorinated solvents: their advantages, disadvantages, and alternatives in organic and medicinal chemistry, Chem. Rev. 121 (2021) 1582–1622, https://doi.org/10.1021/acs.chemrev.0c00709.
[7] Z. Shariatinia, Z. Karimzadeh, Recent advances on oxidation of alcohols over various types of materials as effective catalysts: an overview, Coord. Chem. Rev. 526 (2025) 216372, https://doi.org/10.1016/j.ccr.2024.216372.
[8] A. Gavriilidis, A. Constantinou, K. Hellgardt, K.K.M. Hii, G.J. Hutchings, G.L. Brett, S. Kuhn, S.P. Marsden, Aerobic oxidations in flow: opportunities for the fine chemicals and pharmaceuticals industries, React. Chem. Eng. 1 (2016) 595–612, https://doi.org/10.1039/C6RE00155F.
[9] P.T. Anastas, J.C. Warner, J.C. Warner, Green Chemistry: Theory and Practice, 1. Paperback, Oxford University Press, Oxford, 2000.
[10] C. Parmeggiani, C. Matassini, F. Cardona, A step forward towards sustainable aerobic alcohol oxidation: new and revised catalysts based on transition metals on

solid supports, Green Chem. 19 (2017) 2030–2050, https://doi.org/10.1039/c7gc00406k.
[11] Z. Shi, C. Zhang, C. Tang, N. Jiao, Recent advances in transition-metal catalyzed reactions using molecular oxygen as the oxidant, Chem. Soc. Rev. 41 (2012) 3381, https://doi.org/10.1039/c2cs15224j.
[12] C. Wang, J. Xiao, Activation of molecular oxygen and selective oxidation with metal complexes, Acc. Chem. Res. 58 (2025) 714–731, https://doi.org/10.1021/acs.accounts.4c00731.
[13] R. Noyori, M. Aoki, K. Sato, Green oxidation with aqueous hydrogen peroxide, Chem. Commun. (2003) 1977, https://doi.org/10.1039/b303160h.
[14] X.-F. Wu, J.-L. Gong, X. Qi, A powerful combination: recent achievements on using TBAI and TBHP as oxidation system, Org. Biomol. Chem. 12 (2014) 5807–5817, https://doi.org/10.1039/C4OB00276H.
[15] X. Hu, M. Fan, Y. Zhu, Q. Zhu, Q. Song, Z. Dong, Biomass-derived phosphorus-doped carbon materials as efficient metal-free catalysts for selective aerobic oxidation of alcohols, Green Chem. 21 (2019) 5274–5283, https://doi.org/10.1039/C9GC01910C.
[16] J. Sánchez, M.D. Curt, N. Robert, J. Fernández, Biomass resources, in: Role Bioenergy Bioeconomy, Elsevier, 2019, pp. 25–111, https://doi.org/10.1016/B978-0-12-813056-8.00002-9.
[17] S.D. Tetali, Terpenes and isoprenoids: a wealth of compounds for global use, Planta 249 (2019) 1–8, https://doi.org/10.1007/s00425-018-3056-x.
[18] P. Pal, A.K. Shaw, The evolution of comprehensive strategies for furanoid glycal synthesis and their applications, RSC Adv. 7 (2017) 25897–25963, https://doi.org/10.1039/C6RA28598H.
[19] S. Serra, D. De Simeis, Two complementary synthetic approaches to the enantiomeric forms of the chiral building block (2,6,6-Trimethyltetrahydro-2H-pyran-2-yl)methanol: application to the stereospecific preparation of the natural flavor Linaloyl oxide, Catalysts 8 (2018) 362, https://doi.org/10.3390/catal8090362.
[20] I. Larrosa, P. Romea, F. Urpí, Synthesis of six-membered oxygenated heterocycles through carbon–oxygen bond-forming reactions, Tetrahedron 64 (2008) 2683–2723, https://doi.org/10.1016/j.tet.2007.11.092.
[21] T. Noguchi, Y. Hirai, M. Kirihara, Highly selective 30% hydrogen peroxide oxidation of sulfides to sulfoxides using micromixing, Chem. Commun. (2008) 3040, https://doi.org/10.1039/b802502a.
[22] J.G. Urones, D. Díez, I.S. Marcos, P. Basabe, A.M. Lithgow, R.F. Moro, N. M. Garrido, R. Escarcena, The use of acyclic monoterpenes in the preparation of β-pyrones: synthesis of the right-hand fragment of Usneoidone E, Tetrahedron 51 (1995) 3691–3704, https://doi.org/10.1016/0040-4020(95)00084-L.
[23] I. Bombarda, L. Cezanne, E.M. Gaydou, Epoxidation–cyclization of rosewood oxides, flavour, Fragr. J. 19 (2004) 275–280, https://doi.org/10.1002/ffj.1311.
[24] C.B. Vilanculo, M.J. Da Silva, M.G. Teixeira, J.A. Villarreal, One-pot synthesis at room temperature of epoxides and linalool derivative pyrans in monolacunary $Na_7PW_{11}O_{39}$ -catalyzed oxidation reactions by hydrogen peroxide, RSC Adv. 10 (2020) 7691–7697, https://doi.org/10.1039/D0RA00047G.
[25] A.A.H. Haidar, D. Agustin, Role of organic solvent and influence of oxidant in the oxidation of linalool catalyzed by molybdenum and vanadium complexes, Tetrahedron Green Chem 2 (2023) 100029, https://doi.org/10.1016/j.tgchem.2023.100029.
[26] S.-S. Wang, G.-Y. Yang, Recent advances in polyoxometalate-catalyzed reactions, Chem. Rev. 115 (2015) 4893–4962, https://doi.org/10.1021/cr500390v.
[27] Y. Ishii, K. Yamawaki, T. Ura, H. Yamada, T. Yoshida, M. Ogawa, Hydrogen peroxide oxidation catalyzed by heteropoly acids combined with cetylpyridinium chloride. Epoxidation of olefins and allylic alcohols, ketonization of alcohols and diols, and oxidative cleavage of 1,2-diols and olefins, J. Organomet. Chem. 53 (1988) 3587–3593, https://doi.org/10.1021/jo00250a032.
[28] L. Liu, C. Chen, X. Hu, T. Mohamood, W. Ma, J. Lin, J. Zhao, A role of ionic liquid as an activator for efficient olefinepoxidation catalyzed by polyoxometalate, New J. Chem. 32 (2008) 283–289, https://doi.org/10.1039/b710444h.
[29] B. Guérin, D.M. Fernandes, J.-C. Daran, D. Agustin, R. Poli, Investigation of induction times, activity, selectivity, interface and mass transport in solvent-free epoxidation by H2O2 and TBHP: a study with organic salts of the [PMo12O40]3− anion, New J. Chem. 37 (2013) 3466, https://doi.org/10.1039/c3nj00523b.
[30] N.V. Maksimchuk, O.A. Kholdeeva, K.A. Kovalenko, V.P. Fedin, MIL-101 supported polyoxometalates: synthesis, characterization, and catalytic applications in selective liquid-phase oxidation, Isr. J. Chem. 51 (2011) 281–289, https://doi.org/10.1002/ijch.201000082.
[31] A. Tarlani, M. Abedini, A. Nemati, M. Khabaz, M.M. Amini, Immobilization of Keggin and Preyssler tungsten heteropolyacids on various functionalized silica, J. Colloid Interface Sci. 303 (2006) 32–38, https://doi.org/10.1016/j.jcis.2006.07.024.
[32] Y. Wang, F. Gayet, P. Guillo, D. Agustin, Organic solvent-free olefins and alcohols (ep)oxidation using recoverable catalysts based on [PM12O40]3− (M = Mo or W) ionically grafted on amino functionalized silica nanobeads, Materials 12 (2019) 3278, https://doi.org/10.3390/ma12203278.
[33] R. Zhang, C. Yang, A novel polyoxometalate-functionalized mesoporous hybrid silica: synthesis and characterization, J. Mater. Chem. 18 (2008) 2691, https://doi.org/10.1039/b800025e.
[34] J. Pisk, D. Agustin, R. Poli, Organic salts and Merrifield resin supported [PM12O40]3− (M = Mo or W) as catalysts for adipic acid synthesis, Molecules 24 (2019) 783, https://doi.org/10.3390/molecules24040783.
[35] A.A.H. Haidar, P. Guillo, D. Agustin, Polyoxometalates surrounded by organic cations or immobilized on functionalized Merrifield resin as catalysts for oxidation of β-myrcene and β-caryophyllene, Appl. Sci. 15 (2025) 7981, https://doi.org/10.3390/app15147981.
[36] C.N. Kato, A. Tanabe, S. Negishi, K. Goto, K. Nomiya, An efficient PMo11VVO404−/silica material having cationic ammonium moiety: synthesis, characterization, and catalytic performance for oxidation of alcohols with dioxygen, Chem. Lett. 34 (2005) 238–239, https://doi.org/10.1246/cl.2005.238.
[37] S.A. Dharaskar, M.N. Varma, D.Z. Shende, C.K. Yoo, K.L. Wasewar, Synthesis, characterization and application of 1-Butyl-3 methylimidazolium chloride as green material for extractive desulfurization of liquid fuel, Sci. World J. 2013 (2013) 395274, https://doi.org/10.1155/2013/395274.
[38] G.M. Sheldrick, *SHELXT*– integrated space-group and crystal-structure determination, Acta Crystallogr. Sect. Found. Adv. 71 (2015) 3–8, https://doi.org/10.1107/s2053273314026370.
[39] G.M. Sheldrick, Crystal structure refinement with*SHELXL*, Acta Crystallogr. Sect. C Struct. Chem. 71 (2015) 3–8, https://doi.org/10.1107/s2053229614024218.
[40] G.A. Tsigdinos, C.J. Hallada, Molybdovanadophosphoric acids and their salts. I. Investigation of methods of preparation and characterization, Inorg. Chem. 7 (1968) 437–441.
[41] A.S. Amarasekara, O.S. Owereh, Synthesis of a sulfonic acid functionalized acidic ionic liquid modified silica catalyst and applications in the hydrolysis of cellulose, Catal. Commun. 11 (2010) 1072–1075, https://doi.org/10.1016/j.catcom.2010.05.012.
[42] M. Zare, Z. Moradi-Shoeili, P. Esmailpour, S. Akbayrak, S. Özkar, Oxazine containing molybdenum(VI)–oxodiperoxo complex immobilized on SBA-15 as highly active and selective catalyst in the oxidation of alkenes to epoxides under solvent-free conditions, Microporous Mesoporous Mater. 251 (2017) 173–180, https://doi.org/10.1016/j.micromeso.2017.06.002.
[43] S. Brenna, T. Posset, J. Furrer, J. Blümel, ^{14} N NMR and two-dimensional Suspension^{1} H and^{13} C HRMAS NMR spectroscopy of ionic liquids immobilized on silica, Chem. Eur. J. 12 (2006) 2880–2888, https://doi.org/10.1002/chem.200501193.
[44] W. Stöber, A. Fink, E. Bohn, Controlled growth of monodisperse silica spheres in the micron size range, J. Colloid Interface Sci. 26 (1968) 62–69, https://doi.org/10.1016/0021-9797(68)90272-5.
[45] B. Wiredu, A.S. Amarasekara, Synthesis of a silica-immobilized Brönsted acidic ionic liquid catalyst and hydrolysis of cellulose in water under mild conditions, Catal. Commun. 48 (2014) 41–44, https://doi.org/10.1016/j.catcom.2014.01.021.
[46] C.I.C. Crucho, C. Baleizão, J.P.S. Farinha, Functional group coverage and conversion quantification in nanostructured silica by ^{1}H NMR, Anal. Chem. 89 (2017) 681–687, https://doi.org/10.1021/acs.analchem.6b03117.
[47] N. Plumeré, A. Ruff, B. Speiser, V. Feldmann, H.A. Mayer, Stöber silica particles as basis for redox modifications: particle shape, size, polydispersity, and porosity, J. Colloid Interface Sci. 368 (2012) 208–219, https://doi.org/10.1016/j.jcis.2011.10.070.
[48] K. Nozawa, H. Gailhanou, L. Raison, P. Panizza, H. Ushiki, E. Sellier, J.P. Delville, M.H. Delville, Smart control of monodisperse Stöber silica particles: effect of reactant addition rate on growth process, Langmuir 21 (2005) 1516–1523, https://doi.org/10.1021/la048569r.
[49] E.D.H. Mansfield, Y. Pandya, E.A. Mun, S.E. Rogers, I. Abutbul-Ionita, D. Danino, A.C. Williams, V.V. Khutoryanskiy, Structure and characterisation of hydroxyethylcellulose–silica nanoparticles, RSC Adv. 8 (2018) 6471–6478, https://doi.org/10.1039/C7RA08716K.
[50] M.J. Da Silva, P.H. Da Silva Andrade, S.O. Ferreira, C.B. Vilanculo, C.M. Oliveira, Monolacunary K8SiW11O39-catalyzed Terpenic alcohols oxidation with hydrogen peroxide, Catal. Lett. 148 (2018) 2516–2527, https://doi.org/10.1007/s10562-018-2434-0.
[51] N. Mizuno, K. Yamaguchi, K. Kamata, Epoxidation of olefins with hydrogen peroxide catalyzed by polyoxometalates, Coord. Chem. Rev. 249 (2005) 1944–1956, https://doi.org/10.1016/j.ccr.2004.11.019.
[52] C.B. Vilanculo, M.J. Da Silva, Can Brønsted acids catalyze the epoxidation of allylic alcohols with H2O2? With a little help from the proton, the H3PMo12O40 acid did it and well, Mol. Catal. 512 (2021) 111780, https://doi.org/10.1016/j.mcat.2021.111780.
[53] J. Andraos, M. Sayed, On the use of “green” metrics in the undergraduate organic chemistry lecture and lab to assess the mass efficiency of organic reactions, J. Chem. Educ. 84 (2007) 1004, https://doi.org/10.1021/ed084p1004.